Nature Methods

Predicting protein associations with long noncoding RNAs

Matteo Bellucci, Federico Agostini, Marianela Masin & Gian Gaetano Tartaglia

Supplementary Figure 1	Predictions of interactions in the human MRP complex
Supplementary Figure 2	Predictions of interactions in the human RNase P complex
Supplementary Figure 3	Predictions of interactions between PRC2 protein components and *Xist* regions
Supplementary Figure 4	Predictions of interactions between PRC2 protein components and *HOTAIR* regions
Supplementary Table 1	PDB IDs of non-redundant protein-RNA complexes used to train catRAPID
Supplementary Table 2	Coefficients associated with protein and RNA properties
Supplementary Table 3	Parameters of the interaction matrix I
Supplementary Table 4	Composition of the NPInter dataset
Supplementary Table 5	Composition of the Protein-binding (Protein BP), DNA-binding, RNA-binding (RNA BP) datasets
Supplementary Table 6	Human MRP complex: Comparison between catRAPID predictions and experimental data
Supplementary Methods	

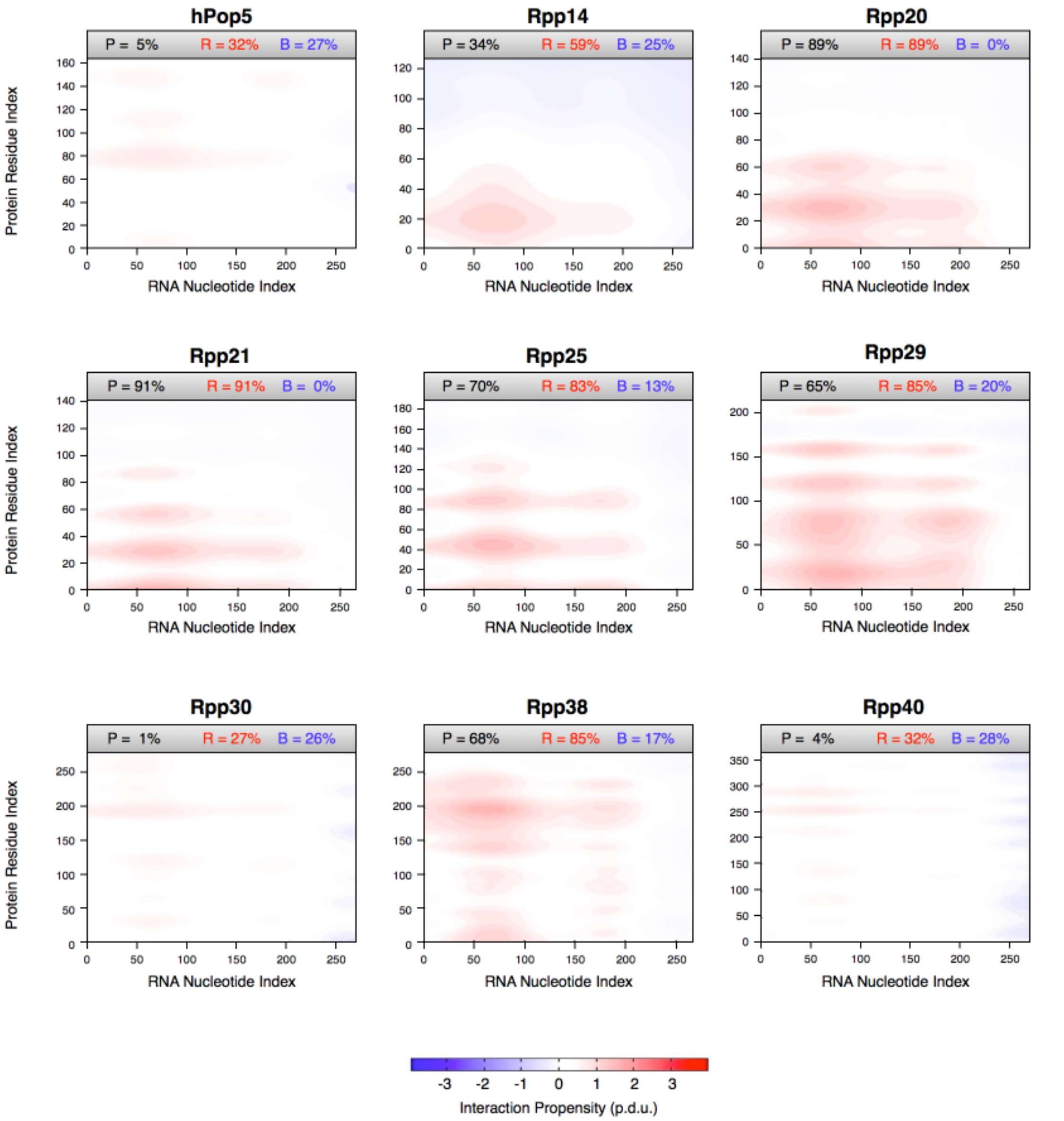

Supplementary Figure 1 *Predictions of interactions in the human MRP complex.* The Interaction propensity score (P) is reported, as well as percentages for positive (R) and negative (B) contributions. See also Supplementary Table 6.

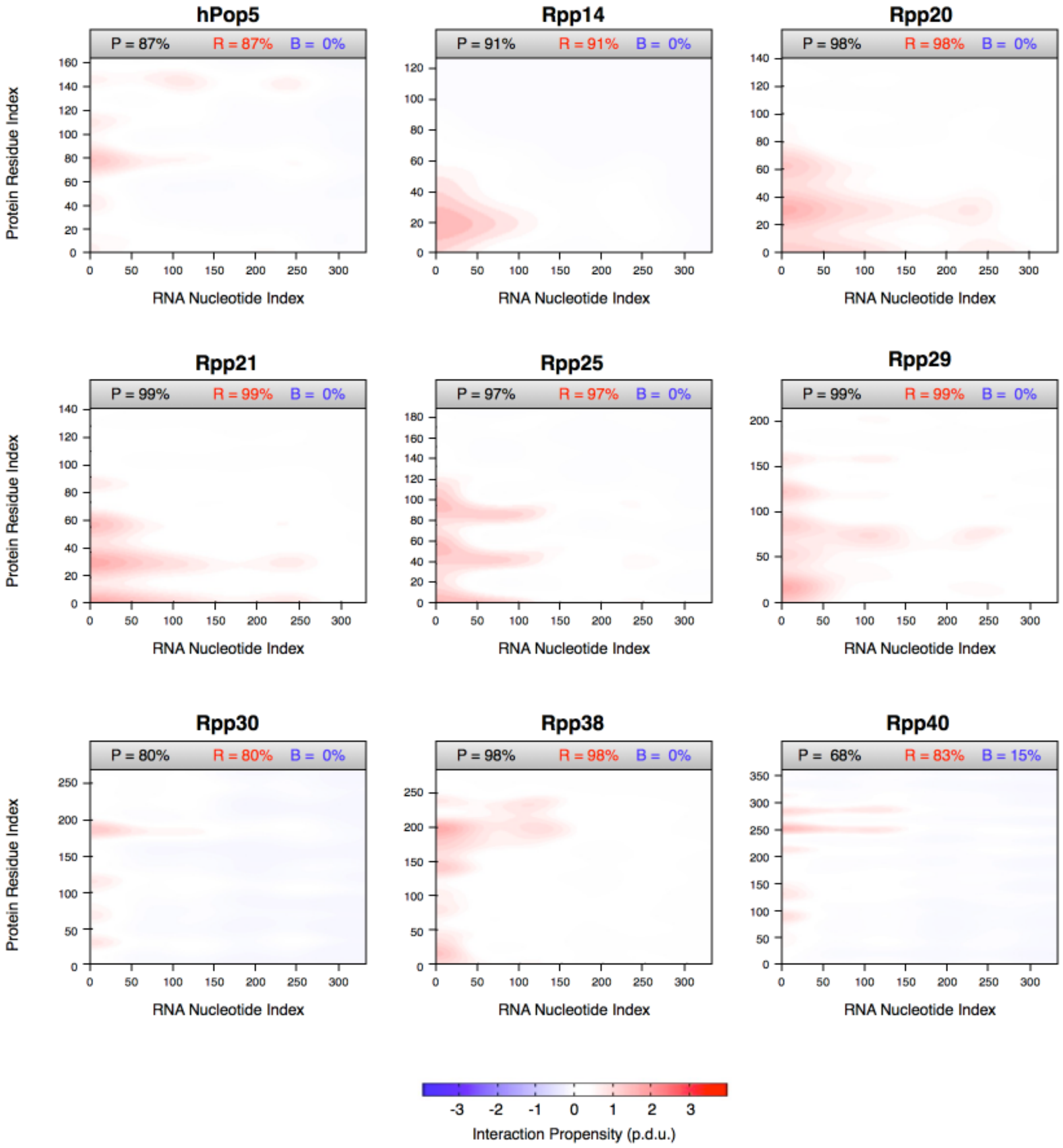

Supplementary Figure 2 *Prediction of interactions in the human RNase P complex.* The Interaction propensity score (P) is reported, as well as percentages for positive (R) and negative (B) contributions. Please refer to the relative section for the interpretation of data.

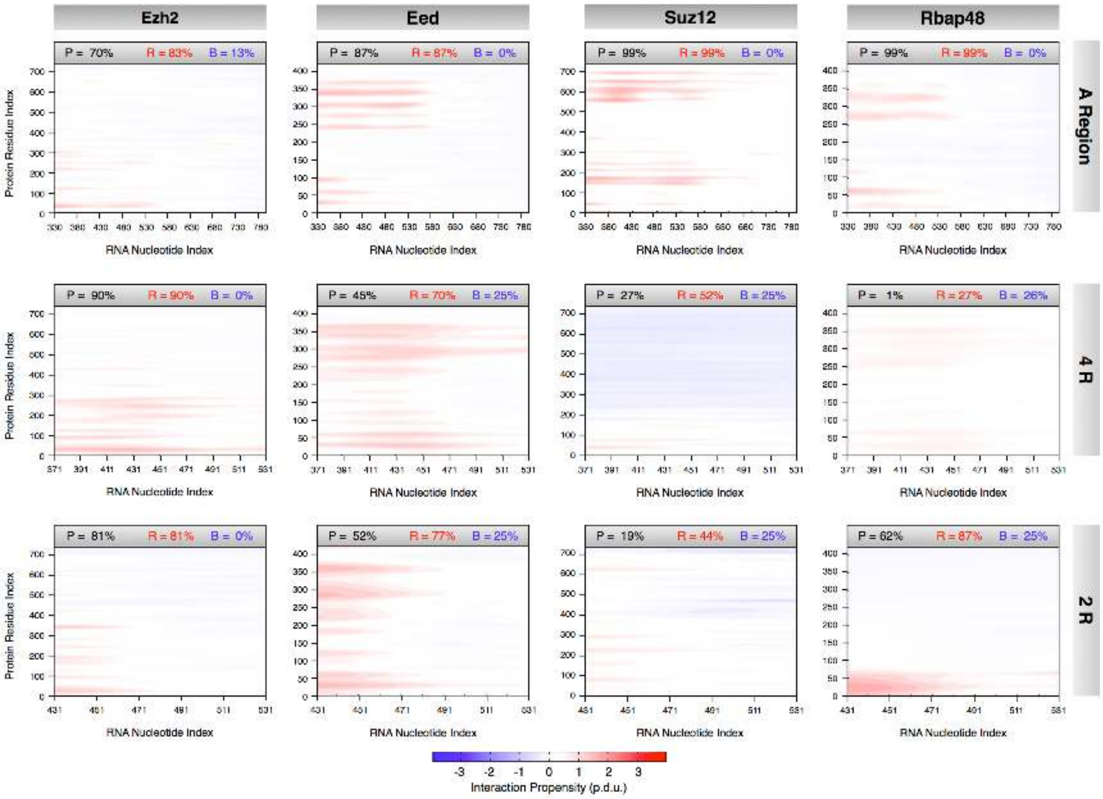

Supplementary Figure 3 *Predictions of interactions between PRC2 protein components and Xist regions*. The Interaction propensity score (P) is reported, as well as percentages for positive (R) and negative (B) contributions.

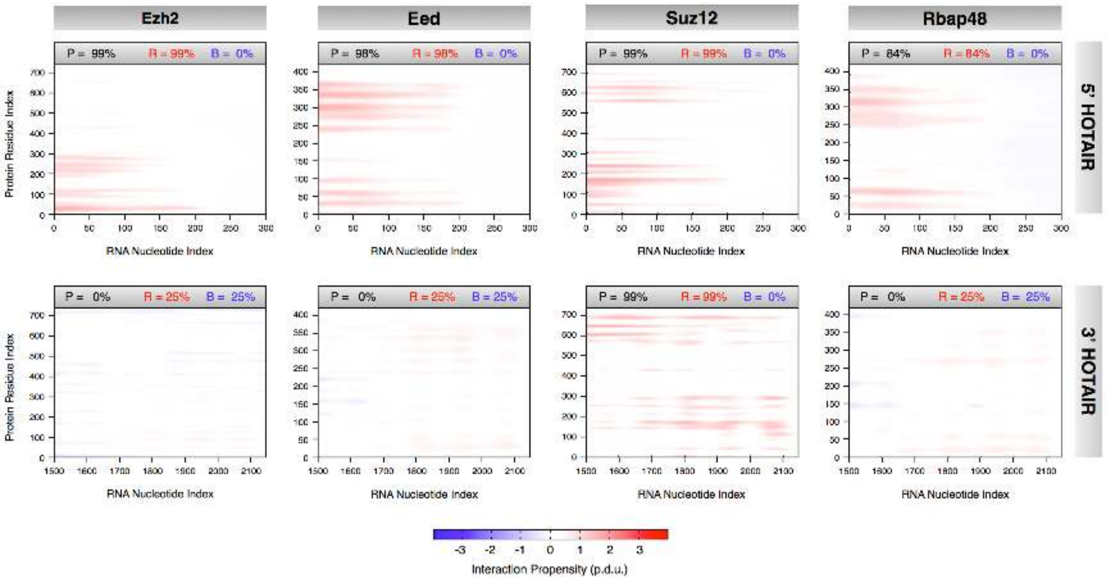

Supplementary Figure 4 *Predictions of interactions between PRC2 protein components and HOTAIR regions.* The Interaction propensity score (P) is reported, as well as percentages for positive (R) and negative (B) contributions.

2ZKR	3CW1	3I8I	2GYA	3BBO	1JJ2	2ZJP	1FFK	1GIY	1P85
3JYV	2GTT	3HUW	3BBN	1C9S	2FTC	2ZKQ	2RKJ	2CZJ	2D6F
3A2K	2ZNI	2WW9	1UN6	1J2B	2NQP	1J5A	3KTW	3EPH	2R8S
2DER	2CT8	1SER	1G59	1ASY	2ZZM	2ZUE	2DU3	1U0B	1J1U
1H3E	1F7U	1EIY	1C0A						

Supplementary Table 1 *PDB codes of non-redundant protein-RNA complexes selected to train catRAPID.* See section **Training Set** for more details**.**

RNA Property	**Coefficients**
Secondary Structure	0.23
Polarity	-0.18
Hydrophobicity	-0.18

Protein Property	**Coefficients**
Alpha Helix	0.27
Beta Sheet	-0.03
Turn / Coil	0.10
Polarity	0.40
Hydrophobicity	-0.22

Supplementary Table 2 *Coefficients associated with protein and RNA properties*.

5.04	-2.07	3.80	4.71	2.12	-0.11	-1.29	0.01	0.67	-2.03
-1.16	5.33	-1.01	1.41	-1.05	3.17	1.33	-0.49	-3.41	4.93
-4.27	0.30	0.22	0.42	0.93	2.49	-1.99	-0.08	1.33	-1.06
9.48	-0.82	1.14	2.64	-3.60	4.88	-2.56	-1.53	0.76	0.80
-2.39	0.96	-1.58	-1.47	3.10	1.37	0.49	0.48	-0.78	-4.63
-0.04	0.56	5.16	0.80	2.18	3.76	0.20	2.24	0.74	5.41
0.98	-2.16	-1.32	-3.79	-3.14	-1.94	2.26	-1.04	0.90	-3.39
2.51	2.91	-3.42	-1.65	1.60	-2.94	-1.30	0.66	1.77	1.19
4.25	1.66	-1.38	-0.32	2.65	-3.99	-2.93	-2.94	-1.85	2.32
-2.54	-0.48	-2.58	0.96	-0.83	3.59	2.17	2.82	-1.50	-3.29

Supplementary Table 3 *Parameters of the interaction matrix I*.

NPInter Class	# Interactions
The ncRNA binds the protein	239
The protein as a factor affects the ncRNA's function	88
The ncRNA is regulated by the protein	22
Special linkages between the ncRNA and the Protein	8
Genetic interaction between the ncRNA gene and the protein	13
The ncRNA regulates the mRNA	24
The ncRNA indirectly regulates a gene (DNA)	9
The ncRNA as a factor affects the protein's function	2

Supplementary Table 4 *Composition of the NPInter dataset*. Indirect evidences of protein-RNA interactions are associated with the following classes: “The ncRNA is regulated by the protein”, “Special linkages between the ncRNA and the Protein”, “Genetic interaction between the ncRNA gene and the protein”, “The ncRNA regulates the mRNA” and “The ncRNA indirectly regulates a gene (DNA)”. See section **Test Set** for more details**.**

Dataset	# Proteins	# Interactions
Protein BP	62	12000
RNA BP	65	12000
DNA BP	5410	130000

Supplementary Table 5 *Composition of the Protein-binding (Protein BP), DNA-binding, RNA-binding (RNA BP) datasets.* For each test set, we generated random associations with RNA molecules present in the training set. See also section **Test Set.**

Protein subunits	catRAPID Predictions		Experimental Evidences		Accordance	References
	P3 stem	P12 stem	P3 stem	P12 stem		
Rpp14	-	-	-	-	YES	
Rpp20	++	+	++	+	YES	13,14
Rpp21	+	+	+	+	YES	
Rpp25	+	+	++	+	YES	13,14
Rpp29	++	++	++	++	YES	
Rpp30	-	-	NA	NA	YES	15
Rpp38	++	++	+	++	YES	
Rpp40	-	-	NA	NA	*	
hPop5	+	-	-	-	YES **	15

Supplementary Table 6 *Human MRP complex: Comparison between experimental data and catRAPID predictions.* The strength of interactions is represented as "++", strong; "+", weak; "-", absent; "NA", not available. Experimental evidences can be found in the work by Welting and collaborators[20], except where differently indicated. *No comparison is possible with experimental data due to lack of information. **Predictions support what shown for the archeal homolog *Pho*Pop5[21].

Supplementary Methods

Training Set

Structural data were collected in March 2010 and consisted of 858 RNA-protein complexes (8367 protein-RNA pairs) available from the RCSB databank (http://www.pdb.org/). A cutoff of 7 Å for physical contacts was employed to discriminate between interacting and non-interacting protein-RNA pairs. The cutoff was decided according to the average resolution of structural complexes and led to define a positive dataset containing 7409 interacting protein-RNA pairs and a negative set containing 958 non-interacting protein-RNA pairs. The CD-HIT tool (http://weizhong-lab.ucsd.edu/cdhit_suite/cgi-bin/index.cgi) was used to filter out RNA and protein sequences with identities higher than 80% and 60%, respectively. After redundancy removal, the database contained 410 interacting ("Positive set") and 182 non-interacting ("Negative set") protein-RNA pairs. With regards to the composition of the Positive and Negative sets, protein-RNA associations were grouped into five functional classes: "Ribosome and protein synthesis", "Splicing", "Transcription", "tRNA synthesis and Viral RNA assemblies", which account for 70%, 10%, 8%, 12% and 10% of the entire training set. Performances were estimated using a ten-fold cross-validation approach, in which a representative set of each functional class was sampled. In the analysis, the data set of interactions was randomly partitioned into ten subsamples requiring the condition that all the partitions carry the same distribution of functional classes. One subsample was retained for testing, and the remaining nine were used for training the algorithm. The cross-validation process was repeated ten times with each of the ten subsamples used exactly once as the validation data. The significance of our predictions was evaluated by calculating p-values (two-tail t-test). See also section **Discriminative Power**.

We tested catRAPID's performance on the identification of binding regions. For each protein-RNA complex in the redundant set, we calculated interaction propensities of all possible associations between amino acid and nucleotide chains and ranked their scores from lowest to highest. Protein binding sites were top-ranked in 87% of cases while RNA binding sites were ranked in 75% of cases. Simultaneous identification of both protein and RNA binding regions was top-ranked in 62% of cases. Indeed, these results underline the extreme accuracy in identifying interaction sites (**Fig. 1a**).

Physico-chemical Properties

Secondary Structure Propensities. The secondary structure of the RNA molecule is predicted from its nucleotide sequence using the Vienna package[1] (including the algorithms RNAfold, RNAsubopt and RNAplot). Although the average predictive power of the RNAfold algorithm is 70%, lower performances are expected for long non-coding RNAs because these transcripts are poorly characterized. To increase the amount of information that can be extracted from secondary structure predictions, we adopted a strategy that exploits the generation of ensembles produced with the RNAsubopt algorithm. The sampling of structures was performed with probabilities estimated through Boltzmann weighting and stochastic backtracking in the partition function. Six model structures, ranked by energy, are used as input for catRAPID. For each model structure, the RNAplot algorithm was employed to generate secondary structure coordinates. Using the coordinates we defined the "secondary structure occupancy" by counting the number of contacts made by each nucleotide within the different regions of the chain. High values of secondary structure occupancy indicate that base pairing occurs in regions with high propensity to form hairpin-loops, while low values are associated with junctions or multi-loops. The secondary structure of proteins was taken into account in our model by calculating the Chou-Fasman[2] and Deleage-Roux[3] propensities for turn, β-strand and α-helical elements. As the average predictive power of these models is around 60%, we preferred to combine together the individual propensities to have better performances. The correlation between interaction propensities and secondary structure contributions is 73% (**Interaction Propensities**).

Hydrogen-Bonding Propensities. The structural information on purine and pyrimidine contacts was extracted from a set of 41 non-redundant protein-RNA complexes[4]. Both the number and the frequency of hydrogen-bond contacts are used in our method. With respect to proteins, we used Grantham's and Zimmerman's scales[5,6] to estimate the propensity of amino acids to form hydrogen bonds. Other propensity scales were disregarded because they showed lower predictive power.

The correlation between interaction propensities and hydrogen bonding contributions is 58% (**Interaction Propensities**).

Van der Waals' Propensities. The information on purine and pyrimidine contacts was taken from a set of 41 protein-RNA complexes[4]. Both the number and the frequency of van der Waals' contacts were used in catRAPID. With respect to proteins, we employed Kyte-Dolittle and Bull-Breese scales[7,8] to estimate the propensity to form van der Waals' contacts. Other propensity scales were disregarded because they showed lower predictive power. The correlation between interaction propensities and Van der Waals' contributions is 26% (estimated with a ten-fold cross-validation).

Fitting coefficients for Secondary Structure, Hydrogen-Bonding and Van der Waals' Contributions are reported in **Supplementary Table 2**.

Interaction Propensity

Secondary structure, hydrogen bonding and van der Waals propensities were combined together into the interaction profile:

$$\left|\Phi_x\right\rangle = \alpha_S\left|S_x\right\rangle + \alpha_H\left|H_x\right\rangle + \alpha_W\left|W_x\right\rangle \qquad (1)$$

We used the symbol $\left|\ \right\rangle$ to indicate the profile associated with a specific physico-chemical property. For example, the van der Waal's profile of a protein is denoted by $\left|W_p\right\rangle$ and contains the van der Waal's contributions of each amino acid:

$$\left|W_p\right\rangle = W_{p\,1},\ W_{p\,2},\ldots,\ W_{p\,L} \qquad (2)$$

Where L is the protein's sequence length. Similarly, $\left|H\right\rangle$ represents the hydrogen bonding profile and $\left|S\right\rangle$ the secondary structure profile. The variable x is used to distinguish between RNA ($x = r$) and protein ($x = p$) profiles.

In order to deal with molecules of different length, we approximated each propensity profile using plane-waves:

$$\tilde{\Phi}_x^k = \sqrt{\frac{2}{length}} \sum_{n=0}^{length} \Phi_x^n \cos\left[\frac{\pi}{length}\left(n+\frac{1}{2}\right)\left(k+\frac{1}{2}\right)\right] \qquad k = 0,1,\ldots L-1 \tag{3}$$

The number of plane waves employed to approximate each profile is L = 50 as the discriminative power does not improve by increasing L.

The following condition was employed to derive the interaction matrix I:

$$\mathrm{I}:\ \max \left\langle \tilde{\Phi}_r \middle| \mathrm{I} \middle| \tilde{\Phi}_p \right\rangle \ \text{ for } (r,p) \in \{\text{positive set}\} \tag{4}$$

The interaction propensity score $\pi = \left\langle \tilde{\Phi}_r \middle| \mathrm{I} \middle| \tilde{\Phi}_p \right\rangle$ is defined as the inner product between the protein profile $\left| \tilde{\Phi}_r \right\rangle$ and the RNA profile $\left| \tilde{\Phi}_p \right\rangle$, weighted by the interaction matrix I:

$$\pi = \left\langle \tilde{\Phi}_r \middle| \mathrm{I} \middle| \tilde{\Phi}_p \right\rangle = \sum_{l,m} \tilde{\Phi}_r^l \, \mathrm{I}_{l,m} \tilde{\Phi}_p^m = \sum_{l,m} \tilde{\Lambda}_{l,m} \tag{5}$$

The interaction propensity matrix $\Lambda_{l,m}$ is obtained by applying Eq. (3) to $\tilde{\Lambda}_{l,m}$.

The interaction matrix I is given by applying Eq. (3) to the parameters $\tilde{\mathrm{I}}_{n,k}$ reported in **Supplementary Table 3**.

Discriminative Power

In order to evaluate the ability of catRAPID to distinguish between interacting and non-interacting RNA-protein associations, we introduced the concept of discriminative power (dp):

$$\mathrm{dp} = \frac{\sum_i \sum_n \vartheta(\pi_i - \pi_n)}{\sum_i \sum_n \vartheta(\pi_i - \pi_n) + \vartheta(\pi_n - \pi_i)} = 1 - (\mathrm{I} \cap \mathrm{N}) \tag{6}$$

Where π_i indicates the interaction propensity of an interacting RNA-protein pairs, π_n represents the interaction propensity of non-interacting molecules, I is the score distribution associated with the positive set and N is the score distribution associated with the negative set. The definition of π is given in the section **Interaction Propensity**. The function $\vartheta(\pi_i - \pi_n)$ is 1 if $\pi_i - \pi_n > 0$ and 0 otherwise. According to the definition given in Eq. (6), the discriminative power ranges from 0% to 100%. The significance of predictions was evaluated by calculating p-values (two-tail t-test).

With regards to catRAPID's performances, the discriminative power associated with the non-redundant training dataset is 78%. The discriminative power associated with the redundant training dataset is 90%. If a consistent number of protein or RNA sequences are moved from the negative to the positive set (or vice-versa), the distribution of interaction propensities associated with the positive and negative sets tend to overlap. When the number of sequences transferred from the negative to the positive set equals half the size of the positive set, dp is 42%. If Fourier's coefficients associated with RNA or protein sequences are scrambled (i.e., their order is modified in a random way), dp is < 50%. If we use the unitary matrix in Eq. 3, the algorithm shows a dp of 65% on the training set, which increases up to 71% when the NPInter dataset is also considered.

Interaction Propensity

Using the score distribution f_n associated with the negative training set, we calculated the probability $p(v) = p(\pi \leq v)$ that the score π takes values less than or equal to v (interaction probability):

$$p(v) = \int_{-\infty}^{v} f_n(\pi) d\pi \tag{7}$$

Similarly, using the score distribution f_p of the positive training set, we estimated the probability that the score π takes values more than or equal to v (non-interaction probability):

$$n(v) = \int_{v}^{\infty} f_p(\pi) d\pi \qquad (8)$$

The two probabilities $p(v)$ and $n(v)$ were then combined together to define the interaction propensity $P(v)$:

$$P(v,x) = \frac{x[1-n(v)]p(v)}{[1-n(v)]p(v)[1-x]+x[1-p(v)]n(n)} \qquad (9)$$

where $x = 0.5$

Test Sets

The NPInter database[9] (http://www.bioinfo.org.cn/NPInter/) was used to evaluate the ability of the algorithm to predict interactions between proteins and long non-coding RNAs. RNA sequences were obtained from the fRNAdb database (http://www.ncrna.org/frnadb/). We excluded micro-RNAs from our analysis because their size significantly differs from that of molecules used for training. The long non-coding database contains 405 interactions from 6 model organisms. Only for a subset of the NPInter database direct physical evidence for protein-RNA interactions is reported (Fig. 1b; class “The ncRNA binds the protein” accounting for 59% of the NPInter dataset and class “The protein as a factor affects the ncRNA's function” accounting for 22% of the NPInter dataset). We also estimated the significance of our predictions on the entire database by calculating p-values (two-tail t-test): 0.04 for class “The ncRNA is regulated by the protein”, 0.21 for class “Special linkage between the ncRNA and the Protein” 0.11 for class “Genetic interaction between the ncRNA gene and the protein”, 0.03 for class “The ncRNA regulates the mRNA”), 0.20 for class “The ncRNA indirectly regulates a gene” and 0.6 for class “The ncRNA as a factor affects the protein's function". The average discriminative power is 85% and was evaluated by comparing the interaction propensities of the different NPInter classes with the interaction propensities of the non-redundant negative set (and increases up to 90% by comparing with the redundant negative set).

The Non-Nucleid-acid-Binding database NNBP[10] was employed to evaluate the ability of catRAPID to identify proteins that have little propensity to interact with RNA molecules. The original set comprises 246 proteins, among which 62 were selected after a search on the Uniprot database (http://www.uniprot.org/) for molecules that are exclusively involved in protein-protein interactions. A total of 12000 random associations were generated with RNA sequences of the positive set. The discriminative power of the algorithm was evaluated by comparing the interaction propensities of the negative set (**Training Set**) with those of the random list. The significance of predictions was evaluated by calculating p-values (two-tail t-test) (Supplementary Table 4).

DNA-binding (DNA BP) and RNA-binding (RNA BP) proteins were obtained from the Uniprot database. DNA BP were collected by searching for molecules that bind "with DNA and not with RNA" (7535 hits), while RNA BP were obtained by selecting molecules that bind "with RNA and not with DNA" (84 hits). The CD-HIT tool was used to filter out sequences with identities higher than 60%. After filtering we counted a total of 5410 entries for DNA BP and 65 entries for RNA BP). Random associations were generated with RNA sequences present in the positive training set (130000 associations for DNA-binding and 12000 for RNA-binding, respectively). The discriminative power of the algorithm was evaluated by comparing interaction propensities of the negative set (**Training Set**) with those of the random lists. The significance of predictions was evaluated by calculating p-values (two-tail t-test) (Supplementary Table 5).

The Human MRP and RNase P Complexes

The human MRP complex is comprised of ten protein subunits (hPop1, hPop5, Rpp14, Rpp20, Rpp21, Rpp25, Rpp29, Rpp30, Rpp38 and Rpp40) and one RNA unit (266 nucleotides). The RNA shows a catalytic core domain with evolutionary conserved structural features in domain I (P1-P3 helices), and a variable portion named domain II (P8, P9, P12, eP19 helices) with unknown function. The human RNase P complex shares protein components with the MRP system. It includes one RNA unit (344 nucleotides) that possesses analogous structural features compared to the *MRP RNA*, with a more extended P12 stem and additional P7, P10, P11 elements. The two complexes display different catalytic activities: MRP mediates the processing of rRNA precursors while RNAse P is required for processing pre-tRNAs in functional tRNAs molecules.

Several studies were carried out to identify protein-RNA interactions in human, yeast and bacterial MRP complexes, using a wide variety of techniques[11]. The most detailed picture of the human system was given by Welting and coworkers[12] who demonstrated, using GST pull-down data, that hPop1, Rpp20, Rpp21, Rpp25, Rpp29 and Rpp38 directly interact with RNA, whereas hPop5 and Rpp14 are part of the assembly but do not contact the transcript. Interaction data for Rpp30 and Rpp40 are missing because of the poor solubility of the proteins. It has been observed that Rpp20 and Rpp25 bind strictly to the P3 helix, whereas Rpp29 mediate additional contacts in the P12 stem by associating with more than one RNA region. The interaction between RNA, Rpp20 and Rpp25 was confirmed by the very recent release of the crystal structure of the *MRP RNA* P3 stem in complex with yeast homologues of Rpp20 and Rpp25[13].

Comparisons between our predictions and experimental evidences can be summarized as follows (**Supplementary Table 6**, **Supplementary Fig. 1**): i) Rpp20 and Rpp21 binds the P3 stem that can be considered a nucleation center. The predicted binding region for Rpp20 - *MRP RNA* corresponds to the one observed in the crystal structure of yeast *MRP RNA* P3 portion in complex with the yeast homolog POP7[13]. ii) Rpp29 and Rpp38 mediate multiple interactions between P3 helix and P12 stem. These results are in complete agreement with the known interaction map of Rpp29 which connects domain I and II[12]. iii) Rpp25 is predicted to have lower propensity to interact with RNA. This finding can be explained by considering that Rpp25 is able to recognize the P3 element of *MRP RNA* only after association with Rpp20[14]. iv) Rpp14, Rpp30 and Rpp40 are predicted to be non-interacting with MRP RNA, in agreement with what was reported in literature[12]. v) hPop5 is predicted to mediate weak interactions with the MRP RNA in the P3 area.

This finding is in accordance with activity assays conducted on the archeal homolog *Pho*Pop5[15].

With regards to the RNase P system, similar interaction propensities were found for Rpp20, Rpp21, Rpp25, Rpp29 and Rpp38 (**Supplementary Fig. 2**). In general, an increase in the intensity of signals is observed together with an enhanced binding preference for the P3 stem region. This finding could be explained by considering the different substrate specificity and catalytic activity of the two RNA-protein assemblies.

Association of the PRC-2 with *Xist* and *HOTAIR*

The Polycomb Repressive Complex is comprised of four protein units: Ezh2, Eed, Suz12 and Rbap48. Ezh2 and Eed are predicted by catRAPID to contact approximately the same RNA regions (330-680 and 330-530 for *Xist* A Region; 1-240 and 1-220 for the 5' domain of *HOTAIR*; **Supplementary Fig. 3**), which is well in agreement with the ability of these proteins to heterodimerize[16]. Eed shows similar binding propensities with both 2R (431-531; **Supplementary Fig. 3**) and 4R (371-531; **Supplementary Fig. 3**) segments, as shown by immuno-precipitation assays[17]. According to previous experimental evidences[18] and in agreement with our predictions on repeat regions, Ezh2 can be regarded as the main RNA-binding subunit, representing the catalytic core of the PCR2 complex. Higher propensity to bind 2R is found for Rbap48, which might arise from its involvement in mediating protein-protein interactions in addition to RNA binding[19].

Databases used for MRP, Xist and HOTAIR

RNA sequences (human *MRP RNA*, FR355912; human *RNase P RNA*, FR174566) were downloaded from the fRNAdb database (http://www.ncrna.org/frnadb/). Protein sequences were retrieved from Uniprot database (hPop5, Q969H6; Rpp14, O95059; Rpp20, O75817; Rpp21, Q9H633; Rpp25, Q9BUL9; Rpp29, O95707; Rpp30, P78346; Rpp38, P78345; Rpp40, O75818). The catRAPID algorithm was employed to predict the interaction propensity of all protein subunits except for hPop1 whose large size does not fit with our computational requirements. The three-dimensional structure of the *MRP* P3 domain in complex with POP6-POP7 was displayed using the UCSF Chimera visualization tool (http://www.cgl.ucsf.edu/chimera/). The crystal structure of the yeast *MRP* P3 domain in complex with the POP6-POP7 protein heterodimer (PDB code: 3iab) was released in July 2010.

The RNA sequences of human *Xist* (M97168.1) and *HOTAIR* (DQ926657.1) were downloaded from the NCBI database. Regions of interest were selected on the basis of available experimental data (sequence numbering is reported): *Xist* A Region, 330-796; *Xist* 4R, 371-531; 5’ *HOTAIR*, 1-300; 3’ *HOTAIR*, 1500-2146. The catRAPID algorithm was used to predict the interaction propensity of the four PRC2 protein subunits, whose Uniprot IDs are: Ezh2, Q15910; Eed, O75530; Suz12, Q15022; Rbap48, Q09028.

References

1. Gruber, A.R., Lorenz, R., Bernhart, S.H., Neubock, R. & Hofacker, I.L. The Vienna RNA Websuite. *Nucleic Acids Research* **36**, W70-W74 (2008).
2. Chou, P.Y. & Fasman, G.D. Prediction of the secondary structure of proteins from their amino acid sequence. *Adv. Enzymol. Relat. Areas Mol. Biol* **47**, 45-148 (1978).
3. Deléage, G. & Roux, B. An algorithm for protein secondary structure prediction based on class prediction. *Protein Eng* **1**, 289-294 (1987).
4. Morozova, N., Allers, J., Myers, J. & Shamoo, Y. Protein-RNA interactions: exploring binding patterns with a three-dimensional superposition analysis of high resolution structures. *Bioinformatics* **22**, 2746-2752 (2006).
5. Grantham, R. Amino acid difference formula to help explain protein evolution. *Science* **185**, 862-864 (1974).
6. Zimmerman, J.M., Eliezer, N. & Simha, R. The characterization of amino acid sequences in proteins by statistical methods. *J. Theor. Biol* **21**, 170-201 (1968).
7. Kyte, J. & Doolittle, R.F. A simple method for displaying the hydropathic character of a protein. *J. Mol. Biol* **157**, 105-132 (1982).
8. Bull, H.B. & Breese, K. Surface tension of amino acid solutions: a hydrophobicity scale of the amino acid residues. *Arch. Biochem. Biophys* **161**, 665-670 (1974).
9. Wu, T. et al. NPInter: the noncoding RNAs and protein related biomacromolecules interaction database. *Nucleic Acids Res* **34**, D150-152 (2006).
10. Stawiski, E.W., Gregoret, L.M. & Mandel-Gutfreund, Y. Annotating nucleic acid-binding function based on protein structure. *J. Mol. Biol* **326**, 1065-1079 (2003).
11. Esakova, O. & Krasilnikov, A.S. Of proteins and RNA: the RNase P/MRP family. *RNA* **16**, 1725-1747 (2010).
12. Welting, T.J.M., van Venrooij, W.J. & Pruijn, G.J.M. Mutual interactions between subunits of the human RNase MRP ribonucleoprotein complex. *Nucleic Acids Res* **32**, 2138-2146 (2004).
13. Perederina, A., Esakova, O., Quan, C., Khanova, E. & Krasilnikov, A.S. Eukaryotic ribonucleases P/MRP: the crystal structure of the P3 domain. *EMBO J* **29**, 761-769 (2010).
14. Hands-Taylor, K.L.D. et al. Heterodimerization of the human RNase P/MRP subunits Rpp20 and Rpp25 is a prerequisite for interaction with the P3 arm of RNase MRP RNA. *Nucleic Acids Res* **38**, 4052-4066 (2010).
15. Tsai, H., Pulukkunat, D.K., Woznick, W.K. & Gopalan, V. Functional reconstitution and characterization of Pyrococcus furiosus RNase P. *Proceedings of the National Academy of Sciences* **103**, 16147 -16152 (2006).
16. Han, Z. et al. Structural basis of EZH2 recognition by EED. *Structure* **15**, 1306-1315 (2007).
17. Maenner, S. et al. 2-D structure of the A region of Xist RNA and its implication for PRC2 association. *PLoS Biol* **8**, e1000276 (2010).

18. Zhao, J., Sun, B.K., Erwin, J.A., Song, J. & Lee, J.T. Polycomb proteins targeted by a short repeat RNA to the mouse X chromosome. *Science* **322**, 750-756 (2008).
19. Qian, Y.W. et al. A retinoblastoma-binding protein related to a negative regulator of Ras in yeast. *Nature* **364**, 648-652 (1993).
20. Welting, T.J., Kikkert, B.J., van Venrooij, W.J. & Pruijn, G.J. Differential association of protein subunits with the human RNase MRP and RNase P complexes. *RNA* **12**, 1373-1382 (2006).
21. Honda, T., Hara, T., Nan, J., Zhang, X. & Kimura, M. Archaeal homologs of human RNase P protein pairs Pop5 with Rpp30 and Rpp21 with Rpp29 work on distinct functional domains of the RNA subunit. *Biosci. Biotechnol. Biochem* **74**, 266-273 (2010).